JBC Papers in Press. Published on May 9, 2017 as Manuscript M116.769802
The latest version is at http://www.jbc.org/cgi/doi/10.1074/jbc.M116.769802

Matrix Gla Protein Deficiency Impairs Nasal Septum Growth Causing Midface Hypoplasia

Juliana Marulanda[1], Hazem Eimar[1],Marc D. McKee[1,2],Michelle Berkvens[1],Valentin Nelea[1],Hassem Roman[3],Teresa Borrás[4],Faleh Tamimi[1],Mathieu Ferron[5],Monzur Murshed[1,3,6]

From the Faculty of Dentistry, McGill University, Montreal, H3A1G1, Canada[1], Department of Anatomy and Cell Biology, Faculty of Medicine, McGill University, Montreal, H3A0C7, Canada[2], Division of Experimental Medicine, Department of Medicine, McGill University, Montreal, H4A3J1, Canada[3], Department of Ophthalmology, School of Medicine, University of North Carolina, Chapel Hill, NC 27516, U.S.A[4], Institut de Recherches Cliniques de Montréal, Montreal, H2W1R7, Canada[5], Shriners Hospital for Children, Montreal, H4A0A9, Canada[6].

Running title: *MGP-deficiency impairs craniofacial development*

To whom correspondence should be addressed: Dr. Monzur Murshed, 1(514)282-8255 monzur.murshed@mcgill.ca

Keywords: Matrix Gla Protein (MGP), nasal septum, midface hypoplasia, chondrocyte, apoptosis, craniofacial development, biomineralization, mouse genetics

ABSTRACT

Genetic and environmental factors may lead to abnormal growth of the orofacial skeleton. In the current study, we investigated the craniofacial abnormalities in a mouse model for Keutel syndrome (KS), a genetic disease caused by loss-of-function mutations in the matrix Gla protein (*MGP*) gene. KS patients show ectopic calcification of cartilaginous tissues and impaired midface development. Our comparative cephalometric analyses revealed a severe midface hypoplasia in *Mgp-/-* mice. *In vivo* reporter studies demonstrated that the *Mgp* promoter is highly active at the cranial sutures, cranial base synchondroses and nasal septum. Interestingly, the cranial sutures of the mutant mice appeared normal, and although we observed a mild increase of mineralization at the spheno-occipital synchondrosis, it did not reduce the relative length of the cranial base. Contrary to this, we found the nasal septum to be abnormally mineralized (calcified) and shortened in *Mgp-/-* mice. Transgenic restoration of *Mgp* expression in chondrocytes prevented nasal septum calcification and corrected the craniofacial anomalies caused by MGP deficiency, suggesting a local role for MGP in midface development. Although there was no upregulation of markers for hypertrophic chondrocytes, TUNEL assay showed a marked increase of apoptotic chondrocytes in the calcified nasal septum. Of note, systemic reduction of inorganic phosphate level was sufficient to prevent abnormal mineralization of the nasal septum in *Mgp-/-;Hyp* compound mutants. Our work provides evidence that modulation of local and systemic factors regulating ECM mineralization can be possible therapeutic strategies to prevent ectopic cartilage mineralization and some forms of congenital craniofacial anomalies in humans.

Congenital anomalies or birth defects are a major cause of perinatal lethality, affecting 2-3% of all newborns (1). A significant number of these infants show abnormal craniofacial development that often disrupts the overall body functions and may lead to long-term disabilities (1). Both genetic and epigenetic factors regulating the concerted morphogenesis of two craniofacial tissues, bone and cartilage, may affect the craniofacial growth and patterning. Although the primary causes are genetic, maternal exposure to toxic substances and nutritional status during pregnancy may also lead to these inborn deformities (2–6).

Midface hypoplasia is a developmental

anomaly in which the nasal, maxillary and zygomatic bones in the cheek grow slower than other facial structures (7). Genetic mutations, epigenetic factors or traumatic injuries during the early stage of life may lead to midface hypoplasia (8–11). A mild form of this disorder is usually considered as a harmless developmental anomaly of the face, while a severe form may seriously affect health and well-being. Clinical complications associated with this disease may include sleep apnea, misalignment of the jaws and eyelids, dental malocclusion, chewing and swallowing difficulties, impaired speech and overall disfigurement of the face (12–14) .

Multiple genetic mutations have been associated with craniofacial malformations with severely impaired midface development. For instance, autosomal dominant mutations affecting fibroblast growth factor signaling cause midface hypoplasia in several diseases including Pfeiffer syndrome, Crouzon syndrome and Apert syndrome (8, 15, 16). In these diseases, the primary cause of midface abnormalities is the early fusion of the cranial sutures (craniosynostosis), which is generally associated with the premature closure of the cranial base synchondroses (17, 18).

Although the above developmental anomalies are commonly associated with midface hypoplasia, some rare forms of this disease may have a different etiology that is not yet elucidated. For example, children born to mothers treated with warfarin during pregnancy develop Warfarin embryopathy, a disease characterized mainly by brain haemorrhages and severe midface hypoplasia (6, 9, 19).

Warfarin is a commonly prescribed anticoagulant that inhibits vitamin K epoxide-reductase (VKORC1), which converts the oxidized form of vitamin K_1 to its reduced form. The reduced vitamin K_1 acts as a co-factor for γ-glutamyl carboxylase (GGCX) that is essential for the post-translational gamma-carboxylation of specific glutamic acid residues (Gla) in proteins, collectively known as "Gla proteins"(20). Similarly, patients with mutations in matrix Gla protein (*MGP*) develop Keutel syndrome, a rare genetic disorder primarily characterized by abnormal mineralization (calcification) of all cartilaginous tissues, short stature, stocky distal phalanges, arterial calcification and severe midface hypoplasia (3, 21).

MGP and a related protein, osteocalcin (bone Gla protein, encoded by *Bglap*), are known as skeletal Gla proteins (22). While *Bglap* is expressed specifically by bone-forming osteoblasts, *Mgp* is expressed at high levels by chondrocytes in cartilaginous tissues, vascular smooth muscle cells (VSMCs) in the cardiovascular system and by the endothelial-like cells of the trabecular meshwork (TM) of the eye (23, 24). Although initially, both of these proteins were proposed to be potent inhibitors of extracellular matrix (ECM) mineralization, our previous work demonstrated that only MGP possesses these anti-mineralization functions (22).

MGP-deficient mice (*Mgp-/-* mice) recapitulate most of the phenotypic abnormalities of Keutel syndrome patients, including as recently reported, ectopic arterial calcification (25). However, this latter phenotype is more severe in the mouse model and represents its primary cause of death (26). Although MGP-deficient mice have been well-characterized for their vascular calcification phenotype, their craniofacial anomalies are still understudied.

In the current study, we show that the midface hypoplasia in MGP-deficient mice is primarily caused by the impaired growth of the maxillary and palatine bones associated with abnormal mineralization and shortening of the nasal septum. For the first time, we show the activity of the *Mgp* promoter in the craniofacial complex using an *in vivo* reporter model, and we demonstrate that septal chondrocytes undergo apoptosis in the absence of MGP. Additionally, we show a novel mechanism of cartilage mineralization that, unlike the endochondral bones, does not require differentiated hypertrophic chondrocytes. Also of importance, we demonstrate that the extent of ectopic nasal septum mineralization in MGP-deficiency is phosphate-dependant, where reduction of systemic phosphate levels impedes nasal septum mineralization, preventing craniofacial malformations. Considering their phenotypic similarities to human patients, MGP-deficient mice may be a useful tool to understand the pathology and underlying cause of Keutel Syndrome.

RESULTS

MGP deficiency causes midface hypoplasia. In order to investigate the effects of MGP and osteocalcin (BGLAP) deficiency in craniofacial de-

velopment, the images of lateral and frontal heads of 5-week-old male wild type (WT), *Mgp-/-* and *Bglap-/-* mice were visually examined for gross craniofacial abnormalities. *Mgp-/-* mice showed a severe blunting of the snout and a more rounded and wider face, whereas the *Bglap-/-* mice were indistinguishable from WT mice, as demonstrated by the superimposition of the facial profiles presented in the lateral and frontal images (**Figure 1A-C**). Lateral cephalic X-rays of age- and gender-matched WT, *Mgp-/-* and *Bglap-/-* mice revealed a severe dental malocclusion characterized by an anterior crossbite only in *Mgp-/-* mice; this phenotype was consistent in all the *Mgp*-null mice analyzed. Additionally, we detected an intense radiopaque area above the upper incisors in *Mgp-/-* mice, which was not present in *Bglap-/-* or WT mice (**Figure 1D**, **asterisk and arrow, respectively**). 3D reconstruction of micro-CT scans of the craniofacial complex of WT and *Mgp-/-* mice confirmed the presence of a severe class III malocclusion (overbite) in the mutant mice (**Figure 1E**). Considering the absence of any craniofacial phenotype in *Bglap-/-* mice, we conclude that of these two skeletal Gla proteins, only MGP is essential for normal craniofacial development.

We then performed a detailed cephalometric analysis and found that the maxillary and palatine lengths were more severely affected than other craniofacial structures in the *Mgp-/-* mice. In contrast, the skull height, anterior cranial height and inter-molar maxillary distance were not affected, while only modest decreases were observed in the mandibular measurements (**Figure 2A and B and Supplemental Table S1**). Taken together, these data identify midface hypoplasia as the major craniofacial phenotype in MGP-deficient mice.

Ectopic calcification of the cartilaginous nasal septum in MGP-deficient mice. The aforementioned phenotype called for an understanding of the mechanism by which MGP could affect craniofacial development. As a first step in addressing this question, we studied *Mgp* expression in the craniofacial complex. To that end, we used a 'knock in' model (*Mgp-Cre*) in which a *Cre* recombinase gene has been inserted at the *Mgp* locus after the stop codon (24). These mice were crossed with a reporter transgenic line, *Gtrosa6tm1Sor*, carrying a ubiquitous *Rosa* promoter followed by a 'floxed' insulator sequence and the bacterial β-galactosidase gene. In the resultant compound mutants *Mgp-Cre;Gtrosa6tm1Sor* (referred to hereafter as *Mgp-Cre;LacZ*), the β-galactosidase gene is expressed in tissues where the *Mgp* promoter is active (24). The whole-mount and dissected heads from 2-week-old WT and *Mgp-Cre;LacZ* mice were stained with X-gal for β-galactosidase activity. Intense blue staining revealed *Mgp* promoter expression in all the cranial sutures, more strongly in the lambdoidal and frontonasal sutures (**Figure 3A**). Also, intense β-galactosidase activity was detected in the sphenooccipital synchondrosis (SOS), intersphenoidal synchondrosis (ISS) and in the cartilaginous nasal septum (NS) of the *Mgp-Cre;LacZ* mice (**Figure 3B**).

The lambdoidal, coronal, frontonasal and palatomaxillary sutures were analyzed using 2D micro-CT images, which failed to detect any sign of craniosynostosis or other anomalies in the sutures of *Mgp-/-* mice (**Figure 3C**). Similarly,2D-imaging of micro-CT scans of the SOS and ISS (top panel, sagittal view; lower panel, frontal view) did not detect premature closure of the ISS in these mice. However, at 5 week of age, the SOS appeared to be disorganized with an aberrant pattern of mineralization (**Figure 3D**).

Considering our X-ray analysis showing increased radiopacity in the region corresponding to the nasal septum and the very high expression of *Mgp* promoter in this tissue, we examined its mineralization status in 5-week-old MGP-deficient mice by micro-CT. As presented in **Figure 3E**, frontal sections detected a striking ectopic mineralization of the nasal septum, which normally remains unmineralized throughout life (27).

Von Kossa and van Gieson (VKVG) staining of histological sections showed that although not calcified at birth, by the first week of life, mineral deposition is already detectable in the septal cartilage of MGP-deficient mice. Mineral accumulation then progressively increases as shown by the analyses of septal cartilage of 2- and 5-week-old mutant mice, whereas it remains unmineralized in the WT littermates (**Figure 4**).

Local expression of Mgp in the cartilage corrects the midface hypoplasia in MGP-deficient mice. We next investigated whether the local expression of *Mgp* in chondrocytes is sufficient to correct

the midface hypoplasia in *Mgp-/-* mice. For this purpose, we generated two transgenic lines that expressed *Mgp* under the *Col2a1* promoter (**Figure 5A, top panel**). Semi-quantitative PCR analyses showed higher level of transgene expression in the rib cartilage of one of these founders, although a weak expression of the transgene was also detected in the aorta (**Figure 5A, lower panel**). This observation was further confirmed by quantitative real time PCR (qRT-PCR) (**Figure 5B**). We mated the *Col2a1-Mgp* mice with *Mgp+/-* mice to eventually generate *Mgp-/-,Col2a1-Mgp* mice in the F2 generation. These mice showed approximately a 6-fold increase of *Mgp* expression in the nasal septum when compared to the WT littermates (**Figure 5C**).

In order to examine whether the relative weak expression of *Mgp* transgene in the aorta could prevent arterial calcification, we performed alizarin red staining of the thoracic skeleton and vascular tissues of 5-week-old WT, *Mgp-/-* and *Mgp-/-;Col2a1-Mgp* littermates. We confirmed that the weak expression of the transgene in *Mgp-/-;Col2a1-Mgp* mice was not sufficient to correct the vascular calcification phenotype, suggesting that this is a valid model for our experiments (**Figure 5D**).

We next studied the mineralization status of the nasal septum in *Mgp-/-;Col2a1-Mgp* mice. Histological analyses revealed a complete absence of ectopic mineralization in the septal cartilage. In contrast, the nasal septum of the *Mgp-/-* littermates were severely mineralized (**Figure 5E**). Cephalic X-ray imaging of the *Mgp-/-;Col2a1-Mgp* mice were comparable to that of the WT littermates, confirming a complete correction of the dental and skeletal malocclusion (**Figure 5F**). Similarly, the cranial, maxillary and palatine lengths that were affected in *Mgp-/-* mice, were normalized in the *Mgp-/-;Col2a1-Mgp* mice (**Figure 5G**). Taken together, these data suggest that local expression of MGP by chondrocytes can correct the midface hypoplasia in *Mgp-/-* mice.

MGP-deficient mice have a shorter nasal septum with apoptotic chondrocytes. We next examined the effects of *Mgp* ablation on the growth of the nasal septum. The exposed septal cartilages of WT and *Mgp-/-* littermates were stained with Safranin O, and the longitudinal lengths were measured. There was a significant reduction in the length of the nasal septum of *Mgp-/-* mice (**Figure 6A**). We then analyzed 2D micro-CT images to measure the rostral, basicranial and total skull lengths in WT and *Mgp-/-* mice following previously determined landmarks (28) (**Figure 6B, left panel and Supplemental Table S2**).The rostral (point 1-2) and basicranial (point 2-3, 3-4 and 4-5) lengths were measured and individually normalized by the total cranial length (point 1-5). We found that the rostral segment, but none of the basicranial lengths measured, were shorter in *Mgp-/-* mice (**Figure 6B, right panel**). This result further suggests that the shortening of the nasal septum is the cause of the hypoplastic maxilla in *Mgp-/-* mice.

In order to understand the cause of nasal septum shortening in *Mgp-/-* mice, we first assessed the cell size by calculating the average chondrocyte area. We did not observe any difference between WT and *Mgp-/-* septal chondrocytes (**Figure 7A**). Then, we evaluated chondrocyte proliferation and apoptosis. Anti-Ki67 immunostaining showed a comparable cell proliferation rate between WT and *Mgp-/-* nasal septum chondrocytes (**Figure 7B**). However, we observed an increase of TUNEL positive immature chondrocytes in the calcified nasal septum of *Mgp-/-* mice (**Figure 7C**).

Chondrocyte hypertrophy is not a prerequisite for nasal septum calcification in MGP-deficient mice. We afterwards interrogated whether ectopic nasal septum calcification in *Mgp-/-* mice is analogous to growth plate cartilage mineralization, a physiologic event that occurs during endochondral bone development. First, we compared the expression of a general chondrogenic marker *Col2a1* (encodes type II collagen) in the nasal septum of 1-week-old WT and *Mgp-/-* mice; there was no detectable difference in mRNA levels (**Figure 8A**). Similarly, there was a comparable deposition of type II collagen as evident by immunostaining of the histological sections of the septal cartilage from 2-week-old WT and *Mgp-/-* mice (**Figure 8B**). Interestingly, although the cartilaginous ECM was mineralized, there was no upregulation of the hypertrophic chondrocyte marker *Col10a1* by qRT-PCR analysis, nor was there any alteration of the encoded protein type X collagen when analyzed by immunostaining (**Figure 8C and 8D**). Also, we did not detect any increase of alkaline phosphatase activity, a hallmark of chondrocyte hypertrophy, in the tissue extracts or histological

sections prepared from *Mgp-/-* septal cartilage in comparison to that of WT cartilage (**Figure 8E and 8F**).

Amorphous calcium phosphate as a prominent mineral species in MGP-deficient nasal septum. Ultrastructural analysis of *Mgp-/-* calcified nasal septa by transmission electron microscopy showed globular structures in the ECM, in the vicinity of the chondrocytes. We observed incremental growth lines at the peripheral regions of the deposited mineral (**Figure 9A**). Detailed characterization of the mineral deposits by energy-dispersive X-ray spectroscopy identified them to contain abundant calcium and phosphorus (**Figure 9B**). X-ray diffraction (**Figure 9C**) and electron diffraction (inset in Figure 9C) revealed that the inorganic mineral present in the MGP-deficient nasal septa was primarily an amorphous calcium-phosphate phase, with a slight degree of crystallization towards an apatitic mineral phase as demonstrated by diffraction rings/spectra labelled 1 and 2 (**Figure 9C**). It was also noted that matrix vesicles which are normally present in the mineralizing growth plates, were generally not observed in the calcified nasal septum.

Prevention of nasal septum mineralization in Mgp-/-;Hyp mice. In order to understand whether ectopic mineralization in the nasal septum is regulated by global mechanisms that control bone and cartilage mineralization, we generated *Mgp-/-;Hyp* compound mutants. *Hyp* mice show an approximately 50% reduction of phosphate levels in the serum, with poor bone and tooth mineralization, largely being attributable to this low level of circulating phosphate, otherwise required for appropriate mineralization of the skeleton and dentition (29). As we reported previously, the systemic reduction of phosphate level persists in *Mgp-/-;Hyp* mice, while the serum calcium level was not affected (30) (**Figure 10A**). We performed 3D micro-CT on 5-week-old WT, *Mgp-/-* and *Mgp-/-;Hyp* heads, which revealed a complete absence of cartilaginous nasal septum mineralization in the double mutants (**Figure 10B**). These findings were further confirmed by histology of nasal septum sections demonstrating a complete absence of mineralized ECM in *Mgp-/-;Hyp* mice (**Figure 10C**). Interestingly, there was no TUNEL-positive nuclei detected on the septal sections of *Mgp-/-;Hyp* mice (**Figure 10D**). Cephalometric analyses of micro-CT images showed a correction of the class III malocclusion, together with a normal maxillary and palatine lengths (**Figure 10E and F**). Although there was a significant increase of the cranial length in *Mgp-/-;Hyp* mice in comparison to *Mgp-/-* mice, it remained shorter when compared to that of WT mice (**Figure 10F**).

DISCUSSION

Cephalometric analyses of *Mgp-/-* heads at 5-week-old revealed severe midface abnormalities. Until now, these abnormalities were not fully characterized and the underlying cause of this phenotype was unknown. Interestingly, the facial morphology of this mouse model closely resembles that of Keutel syndrome and Warfarin embryopathy patients, which justifies a thorough mechanistic study of this pathology.

Our micro-CT analyses clearly identified the key features of the facial phenotype in MGP-deficient mice. These measurements suggest that overall; the craniofacial bones are undersized in the mutant mice, which is expected considering their stunted growth. However, the maxilla and palatine bones are disproportionately smaller affecting the overall anteroposterior length. Taken together, the cephalometric analyses confirm that midface hypoplasia is the major cause of craniofacial defects in MGP-deficient mice.

As evident in the published literature, the two major causes of midface hypoplasia are premature cranial base synchondroses fusion, and craniosynostosis – premature closure of the cranial vault sutures (17). It is now believed that the sutures play a passive role during the growth of the craniofacial complex, whereas the synchondroses act as growth centers, providing sites for rapid bone growth until fusion. Particularly, the spheno-occipital synchondrosis has been shown to play a major role as its late ossification and the closure timing correlates with the severity of the midface hypoplasia seen in syndromic patients (17, 28, 31, 32).

Impaired vitamin K metabolism has also been associated with midface hypoplasia. For instance, inactivating mutations in the gene for VKORC1, which generates the reduced form of vitamin K_1, and GGCX, which uses it as a co-factor, both lead to Vitamin K-dependent clotting factor de-

ficiency and midface hypoplasia (33, 34). Similarly, babies born to mothers under anticoagulation therapy with warfarin suffer from Warfarin embryopathy, also showing midface abnormalities (6). Considering that GGCX/VKORC1 mutations or fetal exposure to warfarin both affect gamma carboxylation of Gla proteins, it is expected that these conditions would lead to the inactivation of the skeletal Gla proteins, e.g. MGP and osteocalcin. However, our experimental data presented here show that only MGP, but not osteocalcin deficiency causes midface hypoplasia in mice.

The role of the nasal septum in midface development has been a matter of controversy for over half a century. Scott, in 1951, proposed that the nasal septum, as all other primary cartilages, acts as a growth center, separating the facial structures allowing the sagittal growth of the face (35). This observation was supported by the findings that the nasal septum responds to hormones and growth factors and has an intrinsic ability to grow. Additionally, extirpation of the nasal septum has been shown to impair midface development in rats and rabbits (10, 36). However, such experimental approaches were criticized as facial development is slower in humans than in the animal models used; thus, the observed midface malformations were attributed to the surgical trauma.

In 1968, Moss proposed the nasal septum as a passive structure that serves a supportive role for the other craniofacial structures (37). This notion was challenged by *in vitro* and *in vivo* studies showing that the intrinsic growth capacity of the nasal septum is comparable to that of epiphyseal cartilages (38, 39). Furthermore, the early corrections of nasal septum deformities in infants with cleft lips and palates or other facial defects show a greater effect on the correction of the overall craniofacial irregularities (40). In agreement with these findings, we provide evidence that during the early phases of facial development, ectopic nasal septum mineralization affects the growth of the midface. We report here that the prevention of nasal septum mineralization by transgenic expression of *Mgp* or by systemic reduction of inorganic phosphate levels both corrected the midface abnormalities in MGP-deficient mice. These data support the original theory proposed by Scott that nasal septum acts as a critical growth element during facial development.

We performed an *in vivo* reporter assay to determine *Mgp* promoter activity in the developing craniofacial complex. For this purpose, we used a *Cre* transgenic line in which the gene encoding *Cre* recombinase was 'knocked in' at the *Mgp* locus by placing it directly under the control of the endogenous *Mgp* promoter and its regulatory elements. Crossing this model with the *R26R-lacZ* reporter line enabled us to faithfully establish endogenous *Mgp* expression by following β-galactosidase activity in the resultant offspring (24). The 'knock in' strategy we used is superior to the conventional transgenic approach as the reporter gene expression is not driven by a truncated promoter at a random location in the genome, but by the single copy-endogenous promoter with all its proximal and distal regulatory elements. We found strong *Mgp* promoter activity in the cranial vault sutures, cranial base synchondroses and in the nasal septum. However, our reporter assay only suggests that the promoter is/was active in the β-galactosidase-positive tissues, but does not precisely indicate its time of activity during development. Considering that the cartilaginous part of the nasal septum remains unmineralized throughout adulthood (27), it is likely that *Mgp* is constitutively expressed in this tissue. Collectively, our data from the *in vivo* reporter assay and qRT-PCR gene expression analyses performed at two different time points (2 and 3 weeks of age, respectively) suggest that this is indeed the case.

It is interesting to note that despite the high level of *Mgp* expression in both SOS and ISS, only the SOS growth plates in *Mgp-/-* mice showed mild mineralization irregularities, while the ISS growth plates remained unaffected. In addition, the cranial sutures were also not abnormally mineralized in these mice. The absence of ectopic mineralization at some of these sites could be explained by the action of other mineralization inhibitor(s) (41), which may have differential distributions in various connective tissues. In fact, inorganic pyrophosphate, a potent mineralization inhibitor, may provide complementary anti-mineralization functions in some cartilaginous tissues. This notion is supported by the observation that the severe articular cartilage mineralization caused by impaired pyrophosphate metabolism is absent in MGP-deficient mice (42, 43).

Despite the presence of ectopic mineralization at the SOS, the proportional length of the cranial base was not smaller in *Mgp-/-* skulls. Considering this observation, it is unlikely that the mild ectopic mineralization of the SOS significantly contributed to the disproportionate shortening of the midface. On the other hand, the relative length of the nasal septum as well as the viscerocranium were significantly smaller, suggesting that ectopic mineralization of the septal cartilage is the major cause of midface hypoplasia in MGP-deficient mice.

In order to investigate whether MGP acts locally to prevent abnormal nasal septum mineralization, we generated *Mgp-/-;Col2a1-Mgp* mice. Unexpectedly, the *Col2a1-Mgp* transgene showed a weak expression in the aorta. This can be explained by the positional effects of the transgene integration site in the chromosome alone, or combined effects of both integration site and copy number of the transgene. However, this weak "leaky" expression of the transgene was not sufficient to prevent ectopic mineralization of the arteries in *Mgp-/-;Col2a1-Mgp* mice. Our observation that abnormal nasal septum mineralization was fully prevented despite the presence of mineralized arteries, has two important implications: firstly, it rules out the possibility that the calcified blood vessels adjacent to the nasal septum perichondrium serve as nidi for the observed septal cartilage calcification; and secondly, in agreement with our previous findings, it establishes that MGP acts locally to prevent ectopic calcification (22).

During endochondral bone development, growth plate cartilage mineralization is a normal process that requires chondrocyte hypertrophy, hallmarked by type X collagen expression, and the release of matrix vesicles. Interestingly, chondrocyte hypertrophy and matrix vesicles appear not to be a prerequisite for ectopic mineralization of the cartilaginous ECM in the nasal septum of MGP-deficient mice. This observation suggests that mineral accumulation in the septal cartilage is likely not analogous to growth plate cartilage mineralization, where terminally differentiated chondrocytes undergo hypertrophy, and matrix vesicles seem to participate in the initiation of mineralization (44, 45). We reported a similar nonchondrogenic ectopic mineralization event in the arteries of MGP-deficient mice (46). Based on our observation, we conclude that the initiation of ECM mineralization in the MGP-deficient nasal septum does not require cellular differentiation (nor release of abundant matrix vesicles), but happens spontaneously by calcium phosphate precipitation. As is the case in blood vessels, whether any particular ECM protein promotes this mineral precipitation in the absence of MGP is yet to be determined.

Our analyses of the deposited mineral in the calcified nasal septum of MGP-deficient mice indicate that the mineral is primarily amorphous (non-crystalline) calcium phosphate. This finding indicates that MGP normally influences the early stages of calcium-phosphate precipitation. Although at this point it is not known what structural features in MGP are essential for this function, it may not be solely attributable to the post-translational γ-carboxylation of its glutamic acid residues. Our earlier work showed that osteocalcin, a closely related structural Gla protein, does not possess any significant anti-mineralization function (22). In agreement with this, we did not observe nasal septum mineralization or craniofacial abnormalities in osteocalcin-deficient mice. Recent published *in vitro* data indicate that N-terminal serine residues in MGP undergo phosphorylation and may facilitate the interaction between MGP and hydroxyapatite minerals (47). The *in vivo* significance of these findings is yet to be determined. Identification of the functional residues in MGP is essential to understand the mechanism underlying MGP's anti-mineralization function.

Vascular smooth muscle cells produce large amounts of MGP, which prevents mineralization of the elastic lamina in arterial tissues (46). The vascular mineralization phenotype in MGP-deficient mice is fully penetrant and appears at the same time as the initiation of nasal septum mineralization. This raises the question as to whether mineral deposition in the nasal septum is actually within the blood vessels present in the tissue. However, this possibility can be ruled out by our observation that although the blood vessels are extensively mineralized in *Mgp-/-;Col2a1-Mgp* mice, as is the case in *Mgp-/-* mice, there was no detectable presence of mineral deposits in the septal cartilage of *Mgp-/-;Col2a1-Mgp* mice. Furthermore, although vascular calcification is not reported in most of the Keutel syndrome patients, midface hypoplasia has always been associated with

this disease, suggesting that these two phenotypic traits may not be interrelated.

Our experimental data revealed an increase in apoptosis in the MGP-deficient septal chondrocytes, which may explain, at least in part, the observed shortening of the nasal septum in these mice. Hayano *et al* found that augmented BMP-SMAD signalling leads to apoptosis in the developing nasal cartilage through p53 upregulation (48). Additionally, other laboratories have reported that MGP inhibits BMP signalling in vascular smooth muscle cells (49). Therefore, it is possible that MGP-deficiency in the nasal septum may induce BMP signalling and cause chondrocyte apoptosis. However, this data needs to be confirmed experimentally. A second hypothesis that can explain the increased apoptosis in the nasal septum of *Mgp-/-* mice is the local increase of inorganic phosphate in the cartilaginous ECM. Inorganic phosphate has been shown to be a major regulator of apoptosis of hypertrophic chondrocytes in the developing endochondral bones (50). As reported here, we found the presence of amorphous calcium phosphate precipitates in the calcified nasal septum. The unstable nature of this transient phase may allow the minerals to be readily dissolved, increasing the local inorganic phosphate levels inducing apoptosis of the neighbouring cells. In addition to chondrocytes apoptosis, another possible mechanism that may affect the anteroposterior growth of the nasal septum is the stiffening of its ECM caused by ectopic mineral deposition. Future studies on the mechanical properties of the mineralized septal cartilage will reveal whether this is indeed the case.

Lastly, we found that systemic regulation of inorganic phosphate levels in the serum is sufficient to prevent nasal septum mineralization in *Mgp-/-;Hyp* double mutant mice. Mutations in the *Phex* gene lead to X-linked hypophosphatemia (*Hyp* mice) characterized by phosphaturia and increased osteoid volume. Interestingly, lowering serum phosphate levels in the *Mgp-/-* mice also completely prevents the vascular calcification phenotype, as we reported previously (30). This finding has a substantial clinical implication in that it demonstrates that nasal septum mineralization and craniofacial malformations can be modulated by systemic factors. Future preventive interventions can be developed based on this finding.

EXPERIMENTAL PROCEDURES

Mice: The generation of *Mgp-/-*, *Bglap-/-* (*Ocn-/-*) and *Mgp-Cre;Gtrosa6tm1Sor* mice have already been described (24, 26, 51). All the experiments were performed on mice with C57BL/6 background. *Col2a1-Mgp* transgenic mice were generated by pronuclear injection at the Transgenic Core Facility at the Goodman Cancer Center of McGill University following standard techniques. *Hyp* mice were purchased from Jackson Laboratories. *Mgp-/-;Hyp* double mutants were generated through breeding, and only male mice were used for our analyses. Mice were maintained in a pathogen-free standard animal facility. Genotypes were determined by PCR on genomic DNAs isolated from tail biopsies. The sequences of the primers used for genotyping are provided upon request.

Skeletal preparation: Skeletal tissues from adult mice were fixed overnight in 95% ethanol, stained in 0.015% Alcian Blue dye (Sigma-Aldrich) in a 1:4 solution of glacial acetic acid and absolute ethanol for 24 hours. Tissues were then treated with 2% potassium hydroxide for another 24 hours (or until the soft tissues were dissolved) and then stained by 0.005% Alizarin Red (Sigma-Aldrich) in a 1% potassium hydroxide solution. Finally, the stained skeletal tissues were clarified in 1% potassium hydroxide / 20% glycerol for 2 days.

Radiography and X-ray micro-computed tomography (micro-CT): Radiographic analyses of the mouse heads were performed at the Centre for Bone and Periodontal Research core facility at McGill University, with an XPERT X-ray imaging system (Kubtec). Micro-CT scanning of mouse skulls was performed with a SkyScan model 1072 instrument (SkyScan) set at a resolution of 8.0 μm and 0.5-mm Al filter. Micro-CT image processing and analysis was performed with version 2.2f of the manufacturer's software (SkyScan). Cephalometric measurements, sutures and cranial base analyses were done using the software Data Viewer (SkyScan). The 3D-reconstructions of head scans were done using the CtAn and CtVol software (SkyScan).

Cephalometric analysis: Cephalometric analyses of micro-CT scans of whole heads were done following the method reported by Eimar, *et al* (52). Cephalometric analysis of the basicranium was

done according to the modified method reported by Laurita, *et al* (28). Only male mice were used for the cephalometric and basicranial studies.

Histology and tissue imaging: Mouse skulls were fixed overnight in 10% formalin, embedded in methyl methacrylate, sectioned (7μm), and stained by von Kossa and van Gieson (VKVG) or hematoxylin and eosin for cell size assessment. For type II (ab21291, Abcam Inc) and type X collagen (a generous gift from Dr. Pierre Moffatt, Shriners Hospital for Children, Montreal (53)) and Ki-67 (ab66155 Abcam Inc) immunohistochemistry, 7μm-thick paraffin sections of decalcified tissues were prepared. Hematoxylin (Fisher Diagnostics) was used for visualization of cell nuclei. Images were taken using a light microscope (DM200; Leica Microsystems Inc) with 20X (numerical aperture of 0.40) and 40X (numerical aperture of 0.65) objectives. Exposed cartilaginous nasal septa were stained with Safranin-O (BioShop) and scanned using an Epson V700 PHOTO scanner. Cell area (μm^2) was measured using PhotoShop (Adobe). All histological images were captured using a digital camera (DP72; Olympus Canada Inc), acquired with DP2-BSW software (XV3.0; Olympus Canada Inc), and processed using PhotoShop software (Adobe).

TUNEL assay: Terminal deoxynucleotidyl-transferase-mediated dUTP nick end labeling (TUNEL) assay was performed using a colorimetric (Trevigen) or a fluorometric (Promega) kit following the manufacturer's instructions. Samples from 2- and 3-week-old mice were decalcified in 25% EDTA (Sigma-Aldrich) in PBS and embedded in paraffin to cut 7 micron sections. Upon labeling, sections were counterstained with 1% methyl green or H33258 (Sigma-Aldrich). TUNEL-positive cells were visualized using light (DM200; Leica Microsystems Inc) and fluorescence (EVOS FL Cell Imaging System, ThermoFisher Scientific) microscopes and quantified using Image-J software from NIH.

Alkaline phosphatase activity assay: Tissue extracts were prepared with 1x Passive Lysis Buffer (Promega) and total proteins were measured by the Micro BCA protein assay (Thermo Scientific). Alkaline phosphatase activity was measured using ρ-nitrophenyl phosphate substrate (Sigma-Aldrich) and then normalized by the respective protein concentration in the extracts.

X-gal staining: For 5-Bromo-4-Chloro-3-Indolyl-β-D-Galactopyranoside (X-gal) (BioShop) staining; mouse heads were dissected and fixed for 5 min in 2% formalin and 0.2% glutaraldehyde in PBS containing 5mM EGTA and 2mM $MgCl_2$. Fixed tissues were rinsed with PBS containing 2mM $MgCl_2$ and 0.2% IGEPAL® CA 630 and left 4 hours in the same buffer supplemented with 5mM of $K_3Fe(CN)_6$ and 5mM of $K_4Fe(CN)_{6.3}H_2O$. Later, the whole mount heads were stained for 4 hours at 37°C in 25 mg/mL X-gal diluted in the same buffer.

Gene expression analysis: Gene expression analyses were performed using a quantitative real-time PCR (qRT-PCR) system (Model 7500; Applied Biosystems). Total RNA was extracted from different tissues with TRIZOL reagent (Invitrogen) and subjected to DNase I (Invitrogen) treatment. The first-strand cDNA synthesis and qRT-PCR were performed using a high-capacity cDNA reverse-transcription kit (Applied Biosystems) and Maxima SYBR green quantitative PCR master mix (Fermentas), respectively. Relative gene expression was analyzed using SDS software (Applied Biosystems) using comparative CT and hypoxanthine guanine phosphoribosyl transferase (*Hprt*, a housekeeping gene) expression as an endogenous control. In order to calculate the delta cycle threshold (ΔCT) value, the mean CT value of the expression of a gene in a sample was first normalized to the mean CT value of *Hprt* expression in that sample. The ΔCT value of the calibrator sample was subtracted from that of the sample-of-interest to obtain the $\Delta\Delta$CT value. The relative expression was reported as $2^{-\Delta\Delta CT}$.

Electron microscopy: Ultrastructural characterization was performed by transmission electron microscopy (TEM). Tissues were fixed with 2% glutaraldehyde (Electron Microscopy Sciences) in 0.1 M sodium cacodylate buffer at pH 7.2, followed by dehydration through a series of graded ethanol dilutions. Samples were embedded in LR White acrylic resin (Electron Microscopy Sciences). Ultrathin sections (80nm-thick) were cut using a Leica EM UC6 ultramicrotome (Leica Microsystems Inc), and were placed on formvar-coated nickel grids (Electron Microscopy Sciences) and stained conventionally with uranyl acetate and lead citrate (Electron Microscopy Sciences) for viewing by TEM. A field-emission FEI Tecnai 12 BioTwin TEM (FEI) was

used to image the stained sections at 120 kV.

Electron diffraction: Electron diffraction in the selected-area configuration (SAED) and energy-dispersive X-ray spectroscopy (EDS) were performed at 200 kV with a FEI Tecnai G2 F20 200 cryo-scanning transmission electron microscope equipped with a Gatan Ultrascan 4000 4k x 4k CCD camera system model 895, and an EDAX Octane T Ultra W /Apollo XLT2 SDD and TEAM EDS analysis system (FEI). Samples were as those used for electron microscopy imaging, but sections were left unstained.

X-ray diffraction: X-ray diffraction (XRD) analysis was performed using a D8 Discover diffractometer (Bruker-AXS Inc) equipped with a copper X-ray tube (wavelength, 1.54056 Å) and a HI-STAR general area detector diffraction system mounted on a vertical θ-θ goniometer (Bruker-AXS Inc). Measurements were run in coupled θ–θ scan in microbeam analysis mode (50μm X-ray beam spot size). Samples examined were the same as those used for electron microscopy, where here the microtomed LR White plastic block face (from which TEM sections were obtained) was analyzed directly in the X-ray beam spot mode.

Statistical analysis: All results are shown as means ± standard deviations. Statistical analyses were performed by Student's *t* test or analysis of variance (Tukey's multiple-comparison test) using GraphPad Prism software. *p* values are indicated on the chart when significant.

Study approval: All the animal experiments were performed according to the animal use protocol number 7132 approved by the Animal Care Committee of McGill University.

Acknowledgments: We thank Dr. Gerard Karsenty for critical reading of the manuscript. We also thank Mia Esser, Louise Marineau and Maude Danis Ladouceur for animal husbandry. The core facility for skeletal phenotyping was supported by Le Réseau de Recherche en Santé Buccodentaire et Osseuse (RSBO). This work was supported by operating grants from the Canadian Institutes of Health Research (CIHR) Fund (number 123310 to M.M.). M.M. is an FRQS chercheur-boursier and J.M. received a studentship from RSBO.

Conflict of interest: The authors declare that they have no conflicts of interest with the contents of this article.

Author contributions: JM contributed to the research experimental design, conducted experiments, analyzed data, and prepared the manuscript. HE performed the initial micro-CT scans and cephalometric analysis. MDM conducted the EM, mineral characterization experiments and contributed to manuscript preparation. MB contributed to the analysis of the phenotype of *Mgp-/-;Col2a1-Mgp* mice. VN conducted mineral characterization experiments and proofread the manuscript. HR generated the *Col2a1-Mgp* mice. TB generated the *Mgp-Cre;Gtrosa6tm1Sor* mice. FT contributed to the micro-CT analyses and proofread the manuscript. MF provided the *Bglap-/-* mice and contributed to the experimental design. MM contributed to the research experimental design, conducted experiments, analyzed data and prepared the final version of the manuscript.

REFERENCES

1. WHO, R. M. o. C. A. (2000) Craniofacial anomalies and associated birth defects, *Glob. registry database on craniofacial anomalies*.
2. Wang, Y., Liu, G., Canfield, M. A., Mai, C. T., Gilboa, S. M., Meyer, R. E., Anderka, M., Copeland, G. E., Kucik, J. E., Nembhard, W. N., Kirby, R. S., and National Birth Defects Prevention, N. (2015) Racial/ethnic differences in survival of united states children with birth defects: a population-based study, *J Pediatr* **166**(4), 819–826 e2. 10.1016/j.jpeds.2014.12.025
3. Munroe, P. B., Olgunturk, R. O., Fryns, J. P., Van Maldergem, L., Ziereisen, F., Yuksel, B., Gardiner, R. M., and Chung, E. (1999) Mutations in the gene encoding the human matrix gla protein cause keutel syndrome, *Nat Genet.* **21**(1), 142–4. 10.1038/5102
4. Hur, D. J., Raymond, G. V., Kahler, S. G., Riegert-Johnson, D. L., Cohen, B. A., and Boyadjiev, S. A. (2005) A novel mgp mutation in a consanguineous family: review of the clinical and molecular characteristics of keutel syndrome, *Am J Med Genet. A* **135**(1), 36–40. 10.1002/ajmg.a.30680
5. Lefebvre, M., Dufernez, F., Bruel, A. L., Gonzales, M., Aral, B., Saint-Onge, J., Gigot, N., Desir, J., Daelemans, C., Jossic, F., Schmitt, S., Mangione, R., Pelluard, F., Vincent-Delorme, C., Labaune, J. M., Bigi, N., D'Olne, D., Delezoide, A. L., Toutain, A., Blesson, S., Cormier-Daire, V., Thevenon, J., El Chehadeh, S., Masurel-Paulet, A., Joye, N., Vibert-Guigue, C., Rigonnot, L., Rousseau, T., Vabres, P., Herve, P., Lamaziere, A., Riviere, J. B., Faivre, L., Laurent, N., and Thauvin-Robinet, C. (2015) Severe x-linked chondrodysplasia punctata in nine new female fetuses, *Prenat Diagn*. 10.1002/pd.4591
6. Starling, L. D., Sinha, A., Boyd, D., and Furck, A. (2012) Fetal warfarin syndrome, *BMJ Case Rep* **2012**. 10.1136/bcr-2012-007344
7. Weaver, K. N., El Hallek, M., Hopkin, R. J., Sund, K. L., Henrickson, M., Del Gaudio, D., Yuksel, A., Acar, G. O., Bober, M. B., Kim, J., and Boyadjiev, S. A. (2014) Keutel syndrome: report of two novel mgp mutations and discussion of clinical overlap with arylsulfatase e deficiency and relapsing polychondritis, *Am J Med Genet. A* **164A**(4), 1062–8. 10.1002/ajmg.a.36390
8. Martelli, H., J., Paranaiba, L. M., de Miranda, R. T., Orsi, J., J., and Coletta, R. D. (2008) Apert syndrome: report of a case with emphasis on craniofacial and genetic features, *Pediatr Dent* **30**(6), 464–8.
9. Mehndiratta, S., Suneja, A., Gupta, B., and Bhatt, S. (2010) Fetotoxicity of warfarin anticoagulation, *Arch Gynecol Obstet* **282**(3), 335–7. 10.1007/s00404-010-1369-5
10. Wong, K. K., Filatov, S., and Kibblewhite, D. J. (2010) Septoplasty retards midfacial growth in a rabbit model, *Laryngoscope* **120**(3), 450–3. 10.1002/lary.20769
11. Sarnat, B. G. and Wexler, M. R. (1967) Rabbit snout growth after resection of central linear segments of nasal septal cartilage, *Acta Otolaryngol* **63**(5), 467–78.
12. Patel, N. and Fearon, J. A. (2015) Treatment of the syndromic midface: a long-term assessment at skeletal maturity, *Plast Reconstr Surg* **135**(4), 731e–42e. 10.1097/PRS.0000000000001062
13. Cielo, C. M. and Marcus, C. L. (2014) Obstructive sleep apnoea in children with craniofacial syndromes, *Paediatr Respir Rev*. 10.1016/j.prrv.2014.11.003
14. Hall, B. K. and Precious, D. S. (2013) Cleft lip, nose, and palate: the nasal septum as the pacemaker for midfacial growth, *Oral Surg Oral Med Oral Pathol Oral Radiol* **115**(4), 442–7. 10.1016/j.oooo.2012.05.005
15. Forte, A. J., Alonso, N., Persing, J. A., Pfaff, M. J., Brooks, E. D., and Steinbacher, D. M. (2014) Analysis of midface retrusion in crouzon and apert syndromes, *Plast Reconstr Surg* **134**(2), 285–93. 10.1097/PRS.0000000000000360
16. Chokdeemboon, C., Mahatumarat, C., Rojvachiranonda, N., Tongkobpetch, S., Suphapeetiporn, K., and Shotelersuk, V. (2013) Fgfr1 and fgfr2 mutations in pfeiffer syndrome, *J Craniofac Surg* **24**(1), 150–2. 10.1097/SCS.0b013e3182646454

17. Goldstein, J. A., Paliga, J. T., Wink, J. D., Bartlett, S. P., Nah, H. D., and Taylor, J. A. (2014) Earlier evidence of spheno-occipital synchondrosis fusion correlates with severity of midface hypoplasia in patients with syndromic craniosynostosis, *Plast Reconstr Surg* **134**(3), 504–10. 10.1097/PRS.0000000000000419
18. Paliga, J. T., Goldstein, J. A., Vossough, A., Bartlett, S. P., and Taylor, J. A. (2014) Premature closure of the spheno-occipital synchondrosis in pfeiffer syndrome: a link to midface hypoplasia, *J Craniofac Surg* **25**(1), 202–5. 10.1097/SCS.0000000000000386
19. Howe, A. M., Hawkins, J. K., and Webster, W. S. (2004) The growth of the nasal septum in the 6-9 week period of foetal development–warfarin embryopathy offers a new insight into prenatal facial development, *Aust Dent J* **49**(4), 171–6.
20. Tie, J. K. and Stafford, D. W. (2016) Structural and functional insights into enzymes of the vitamin k cycle, *J Thromb Haemost* **14**(2), 236–47. 10.1111/jth.13217
21. Meier, M., Weng, L. P., Alexandrakis, E., Ruschoff, J., and Goeckenjan, G. (2001) Tracheobronchial stenosis in keutel syndrome, *Eur Respir J* **17**(3), 566–9.
22. Murshed, M., Schinke, T., McKee, M. D., and Karsenty, G. (2004) Extracellular matrix mineralization is regulated locally; different roles of two gla-containing proteins, *J Cell Biol* **165**(5), 625–30. 10.1083/jcb.200402046
23. Luo, G., D'Souza, R., Hogue, D., and Karsenty, G. (1995) The matrix gla protein gene is a marker of the chondrogenesis cell lineage during mouse development, *J Bone Min. Res* **10**(2), 325–34.
24. Borras, T., Smith, M. H., and Buie, L. K. (2015) A novel mgp-cre knock-in mouse reveals an anticalcification/antistiffness candidate gene in the trabecular meshwork and peripapillary scleral region, *Invest Ophthalmol Vis Sci* **56**(4), 2203–14. 10.1167/iovs.15-16460
25. Pelin, A. (2012) Keutel syndrome: A case report with aortic calcification, *Firat Tip Dergisi* **17**(3), 167–169.
26. Luo, G., Ducy, P., McKee, M. D., Pinero, G. J., Loyer, E., Behringer, R. R., and Karsenty, G. (1997) Spontaneous calcification of arteries and cartilage in mice lacking matrix gla protein, *Nat.* **386**(6620), 78–81. 10.1038/386078a0
27. Palhazi, P., Daniel, R. K., and Kosins, A. M. (2015) The osseocartilaginous vault of the nose: anatomy and surgical observations, *Aesthet Surg J* **35**(3), 242–51. 10.1093/asj/sju079
28. Laurita, J., Koyama, E., Chin, B., Taylor, J. A., Lakin, G. E., Hankenson, K. D., Bartlett, S. P., and Nah, H. D. (2011) The muenke syndrome mutation (fgfr3p244r) causes cranial base shortening associated with growth plate dysfunction and premature perichondrial ossification in murine basicranial synchondroses, *Dev Dyn* **240**(11), 2584–96. 10.1002/dvdy.22752
29. Eicher, E. M., Southard, J. L., Scriver, C. R., and Glorieux, F. H. (1976) Hypophosphatemia: mouse model for human familial hypophosphatemic (vitamin d-resistant) rickets, *Proc Natl Acad Sci U S A* **73**(12), 4667–71.
30. Murshed, M., Harmey, D., Millan, J. L., McKee, M. D., and Karsenty, G. (2005) Unique coexpression in osteoblasts of broadly expressed genes accounts for the spatial restriction of ecm mineralization to bone, *Genes Dev* **19**(9), 1093–104. 10.1101/gad.1276205
31. Rosenberg, P., Arlis, H. R., Haworth, R. D., Heier, L., Hoffman, L., and LaTrenta, G. (1997) The role of the cranial base in facial growth: experimental craniofacial synostosis in the rabbit, *Plast Reconstr Surg* **99**(5), 1396–407.
32. Nah, H. D., Koyama, E., Agochukwu, N. B., Bartlett, S. P., and Muenke, M. (2012) Phenotype profile of a genetic mouse model for muenke syndrome, *Childs Nerv Syst* **28**(9), 1483–93. 10.1007/s00381-012-1778-9
33. Tie, J. K., Carneiro, J. D., Jin, D. Y., Martinhago, C. D., Vermeer, C., and Stafford, D. W. (2016) Characterization of vitamin k-dependent carboxylase mutations that cause bleeding and nonbleeding disorders, *Blood* **127**(15), 1847–55. 10.1182/blood-2015-10-677633

34. Watzka, M., Geisen, C., Scheer, M., Wieland, R., Wiegering, V., Dorner, T., Laws, H. J., Gumruk, F., Hanalioglu, S., Unal, S., Albayrak, D., , and Oldenburg, J. (2014) Bleeding and non-bleeding phenotypes in patients with ggcx gene mutations, *Thromb Res* **134**, 856–865.
35. Scott, J. (1956) Growth at facial sutures, *Am J Orthod Dentofac. Orthop* **42**(5), 381–387.
36. Kvinnsland, S. (1974) Partial resection of the cartilaginous nasal septum in rats; its influence on growth, *Angle Orthod* **44**(2), 135–40. 10.1043/0003-3219(1974)044<0135:PROTCN>2.0.CO;2
37. Moss, M. L., Bromberg, B. E., Song, I. C., and Eisenman, G. (1968) The passive role of nasal septal cartilage in mid-facial growth, *Plast Reconstr Surg* **41**(6), 536–42.
38. Copray, J. C. (1986) Growth of the nasal septal cartilage of the rat in vitro, *J Anat* **144**, 99–111.
39. Al Dayeh, A. A., Rafferty, K. L., Egbert, M., and Herring, S. W. (2013) Real-time monitoring of the growth of the nasal septal cartilage and the nasofrontal suture, *Am J Orthod Dentofac. Orthop* **143**(6), 773–83. 10.1016/j.ajodo.2013.01.012
40. Delaire, J. and Precious, D. (1986) Influence of the nasal septum on maxillonasal growth in patients with congenital labiomaxillary cleft, *Cleft Palate J* **23**(4), 270–7.
41. Marulanda, J., Alqarni, S., and Murshed, M. (2014) Mechanisms of vascular calcification and associated diseases, *Curr Pharm Des* **20**(37), 5801–10.
42. Ho, A. M., Johnson, M. D., and Kingsley, D. M. (2000) Role of the mouse ank gene in control of tissue calcification and arthritis, *Sci.* **289**(5477), 265–70.
43. Okawa, A., Nakamura, I., Goto, S., Moriya, H., Nakamura, Y., and Ikegawa, S. (1998) Mutation in npps in a mouse model of ossification of the posterior longitudinal ligament of the spine, *Nat Genet.* **19**(3), 271–3. 10.1038/956
44. Anderson, H. C. (2003) Matrix vesicles and calcification, *Curr Rheumatol Rep* **5**, 222–226.
45. Golub, E. E. (2009) Role of matrix vesicles in biomineralization, *Biochim Biophys Acta* **1790**, 1592–1598.
46. Khavandgar, Z., Roman, H., Li, J., Lee, S., Vali, H., Brinckmann, J., Davis, E. C., and Murshed, M. (2014) Elastin haploinsufficiency impedes the progression of arterial calcification in mgp-deficient mice, *J Bone Min. Res* **29**(2), 327–37. 10.1002/jbmr.2039
47. O'Young, J., Liao, Y., Xiao, Y., Jalkanen, J., Lajoie, G., Karttunen, M., Goldberg, H. A., and Hunter, G. K. (2011) Matrix gla protein inhibits ectopic calcification by a direct interaction with hydroxyapatite crystals, *J Am Chem Soc* **133**(45), 18406–12. 10.1021/ja207628k
48. Hayano, S., Komatsu, Y., Pan, H., and Mishina, Y. (2015) Augmented bmp signaling in the neural crest inhibits nasal cartilage morphogenesis by inducing p53-mediated apoptosis, *Dev.* **142**(7), 1357–67. 10.1242/dev.118802
49. Zebboudj, A. F., Imura, M., and Bostrom, K. (2002) Matrix gla protein, a regulatory protein for bone morphogenetic protein-2, *J Biol Chem* **277**(6), 4388–94. 10.1074/jbc.M109683200
50. Mansfield, K., Rajpurohit, R., and Shapiro, I. M. (1999) Extracellular phosphate ions cause apoptosis of terminally differentiated epiphyseal chondrocytes, *J Cell Physiol* **179**(3), 276–86. 10.1002/(SICI)1097-4652(199906)179:3<276::AID-JCP5>3.0.CO;2
51. Ducy, P., Desbois, C., Boyce, B., Pinero, G., Story, B., Dunstan, C., Smith, E., Bonadio, J., Goldstein, S., Gundberg, C., Bradley, A., and Karsenty, G. (1996) Increased bone formation in osteocalcin-deficient mice, *Nat.* **382**(6590), 448–52. 10.1038/382448a0
52. Eimar, H., Tamimi, F., Retrouvey, J. M., Rauch, F., Aubin, J. E., and McKee, M. D. (2016) Craniofacial and dental defects in the col1a1jrt/+ mouse model of osteogenesis imperfecta, *J Dent Res* **95**(7), 761–8. 10.1177/0022034516637045
53. Lee, E. R., Lamplugh, L., Kluczyk, B., Leblond, C. P., and Mort, J. S. (2009) Neoepitopes reveal the features of type ii collagen cleavage and the identity of a collagenase involved in the transformation of the epiphyses anlagen in development, *Dev Dyn* **238**(6), 1547–63. 10.1002/dvdy.21960

FOOTNOTES

Abbreviations used within the article: MGP:Matrix Gla Protein, VKORC1: Vitamin K epoxide-reductase, GGCX: γ-glutamyl-carboxylase, BGLAP: Bone Gla Protein (osteocalcin), VSMCs: Vascular smooth muscle cells, TM: Trabecular meshwork, ECM: Extracellular matrix, NS: Nasal septum, SOS: Spheno-occipital synchondrosis, ISS: Intersphenoidal synchondrosis, Micro-CT: Micro-computed tomography, 2D: Two-dimensional, 3D: Three-dimensional, TUNEL: terminal deoxynucleotidyltransferase-mediated dUTP nick end labeling, qRT-PCR: Quantitative real time PCR, BMP: Bone morphogenetic protein, TEM: Transmission electron microscopy.

FIGURES

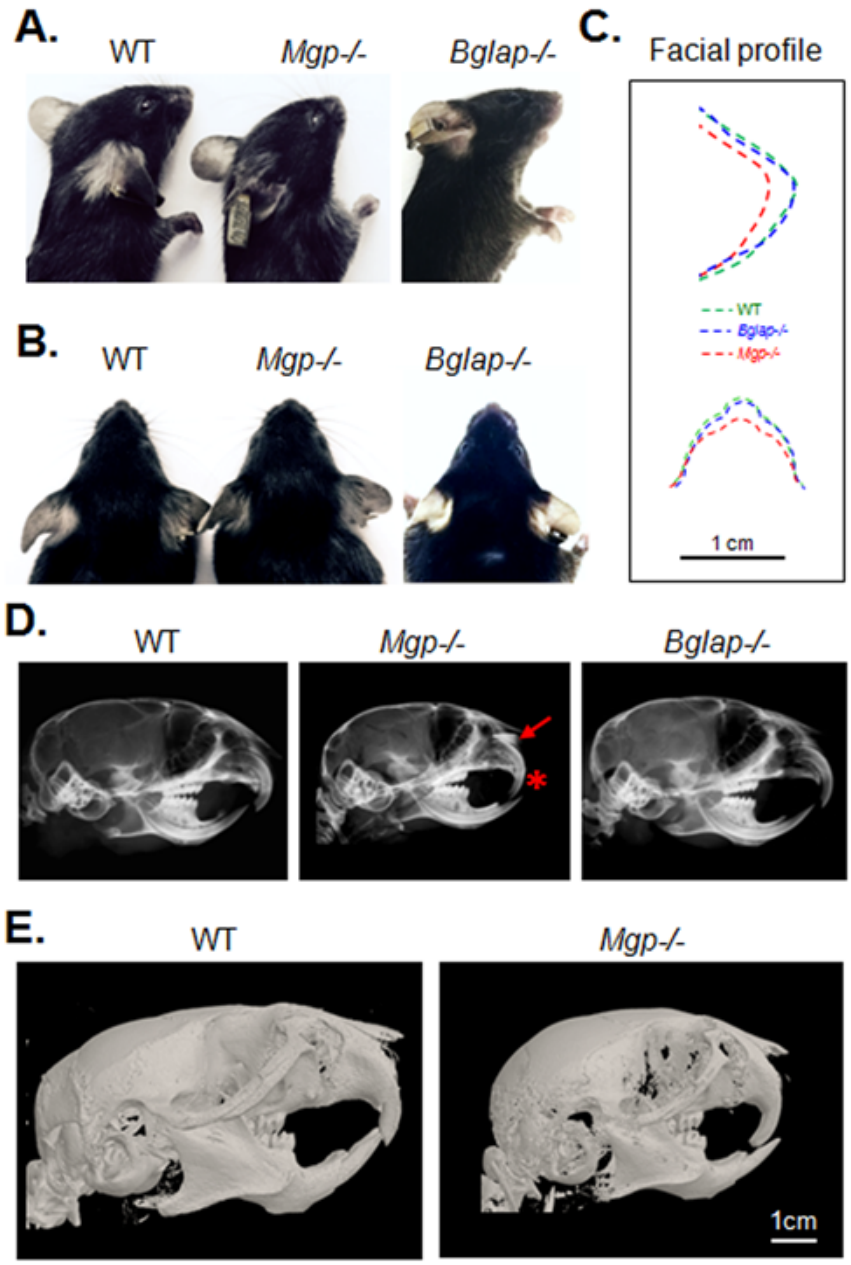

Figure 1: Ablation of *Mgp*, but not *Bglap* causes craniofacial malformations. **A.** Lateral cephalic photographs of WT, *Mgp-/-* and *Bglap-/-* mice showing a blunt and shorter snout in *Mgp-/-* mice. **B.** Frontal cephalic photographs confirming the abnormal craniofacial phenotype in *Mgp-/-* mice. **C.** Superimposition of the lateral and frontal cephalic photographs showing a comparable facial profile between WT and *Bglap-/-* mice and a blunt and wider profile in *Mgp-/-* mice. **D.** Lateral cephalic X-ray of WT, *Mgp-/-* and *Bglap-/-* mice. *Mgp-/-* mice show a severe anterior crossbite with a radiopaque nasal structure (red asterisk and arrow, respectively). **E.** 3D reconstruction of micro-CT scans of WT and *Mgp-/-* mice confirming the dental malocclusion and craniofacial deformities in the latter genotype.

A.

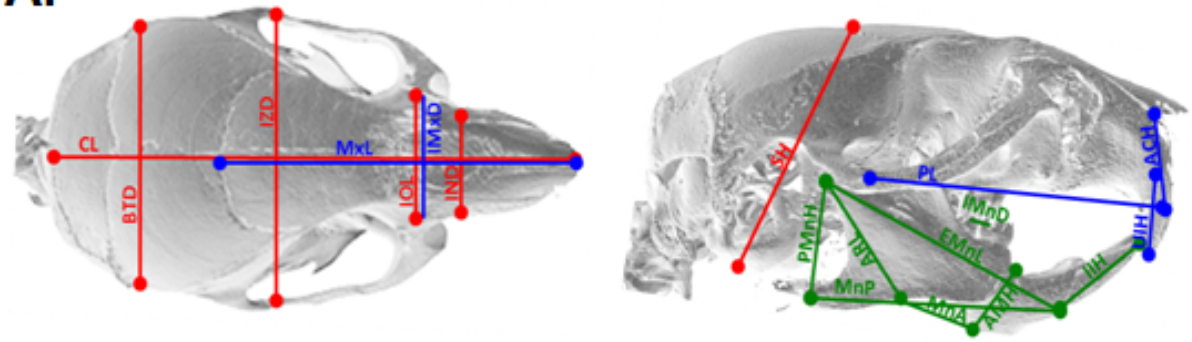

B. Cephalometric analysis

Measurement (mm)	WT	SD	*Mgp-/-*	SD	p
Craniofacial					
Cranial length (CL)	21.94	0.21	19.19	0.23	***
Skull height (SH)	9.01	0.07	8.84	0.06	NS
Inter-nasal distance (IND)	3.45	0.05	3.19	0.08	*
Inter-orbitary length (IOL)	4.2	0.13	4.29	0.11	NS
Inter-zygomatic distance (IZD)	11.96	0.11	11.58	0.1	*
Bi-temporal distance (BTD)	10.13	0.09	9.57	0.11	**
Maxillary					
Maxillary length (MXL)	11.15	0.16	9.2	0.2	***
Palatine length (PL)	12.96	0.14	10.98	0.35	***
Anterior cranial height (ACH)	2.72	0.08	2.68	0.11	NS
Upper incisor height (UIH)	3.2	0.07	3.2	0.1	NS
Inter-molar maxillary distance (IMMD)	3.72	0.03	3.8	0.07	NS
Mandibular					
Effective mandibular length (EML)	10.87	0.12	10.24	0.1	**
Mandibular plane (MNP)	7.14	0.09	6.3	0.07	***
Mandibular axis (MNA)	3.43	0.07	3.14	0.06	*
Inferior incisor height (IIH)	3.83	0.04	3.5	0.08	**
Ascending ramus length (ARL)	5.43	0.1	5.06	0.07	**
Posterior mandibular height (PMNH)	4.91	0.07	4.33	0.07	***
Inter-molar mandibular distance (IMND)	3.9	0.03	3.88	0.07	NS

Figure 2: MGP deficiency causes midface hypoplasia. **A.** Depiction of the selected landmarks for cephalometric analyses of WT and *Mgp-/-* mice. Red, blue and green lines represent the overall craniofacial, maxillary and mandibular measurements, respectively. Description of each landmark's anatomical location is presented in Supplemental Table S1. **B.** Craniofacial, maxillary and mandibular measurements in millimeters. Each value represents the mean of 6 mice analyzed for each genotype at 5-week-old. Statistical analysis: Student's *t* test, SD (Standard deviation).

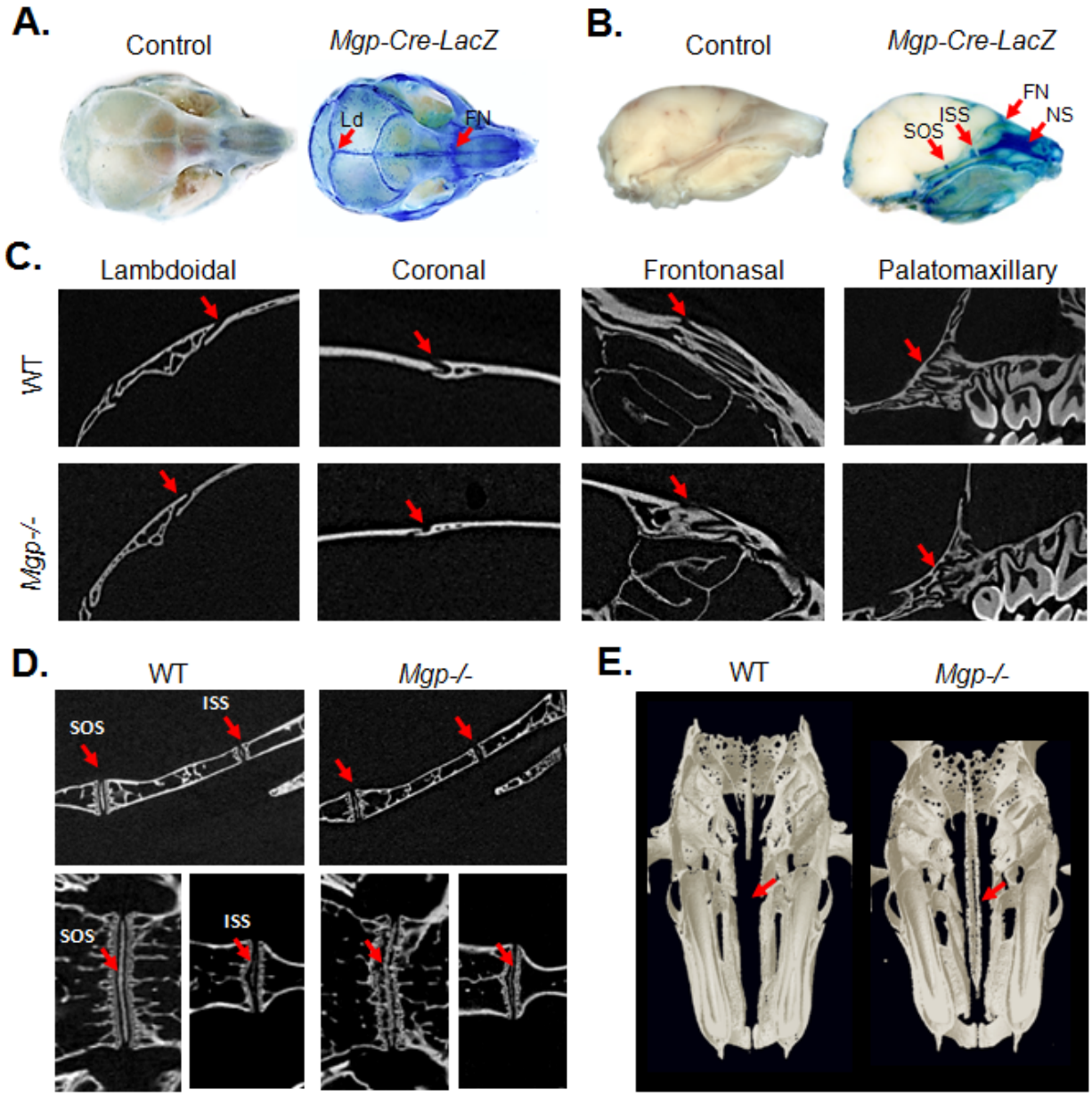

Figure 3: Ectopic calcification of the cartilaginous nasal septum in MGP-deficient mice. A. and **B.** Whole-mount heads of 2-week-old *Mgp-Cre;LacZ* and control mice were stained with X-gal for bacterial β-galactosidase detection. Intense blue staining revealed *Mgp*-promoter activity in all the craniofacial sutures, more intensely in the lambdoidal (Ld) and frontonasal (FN) sutures. The spheno-occipital synchondrosis (SOS), intersphenoidal synchondrosis (ISS) in the basicranial region and nasal septum (NS) were also strongly stained (red arrows; n=3 mice for each group). **C.** 2D images of micro-CT scans of WT and *Mgp-/-* mice showing the absence of craniosynostosis in the mutant mouse in the lambdoidal, coronal, frontonasal and palatomaxillary sutures (red arrows, n=6 in each group). **D.** 2D micro-CT scans (top panels: sagittal view; lower panels: frontal view) of the basicranium of WT and *Mgp-/-* mice showing the normal anatomy of the ISS in the mutant mouse. However, the SOS appeared to be disorganized with an aberrant pattern of mineralization (n=3 mice in each group). **E.** 3D reconstruction of WT and *Mgp-/-* heads in the frontal plane showing a severe nasal septum mineralization in the *Mgp-/-* mice (red arrow, n=6 mice in each group). All the analyses were done on 5-week-old mice unless indicated otherwise.

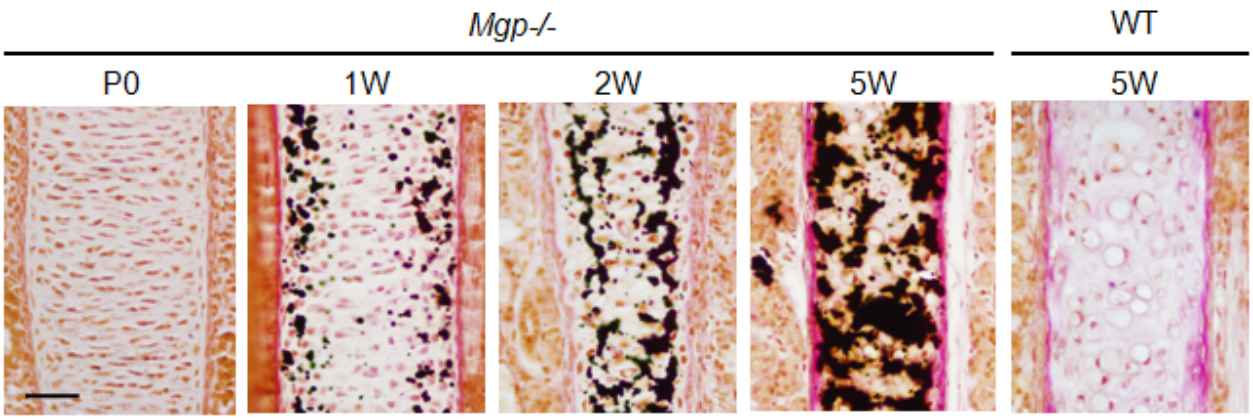

Figure 4: Progressive ectopic mineralization of MGP-deficient nasal septum. Histological analysis of *Mgp-/-* nasal septa by VKVG staining of 7μm-thick plastic sections showing the initiation of pathologic cartilage mineralization at 1 week of age and its progression until 5 weeks of age (n= 3 mice for each time point). The last panel represents an unmineralized WT nasal septum at 5 weeks of age stained with VKVG. Scale bar represents 20μm.

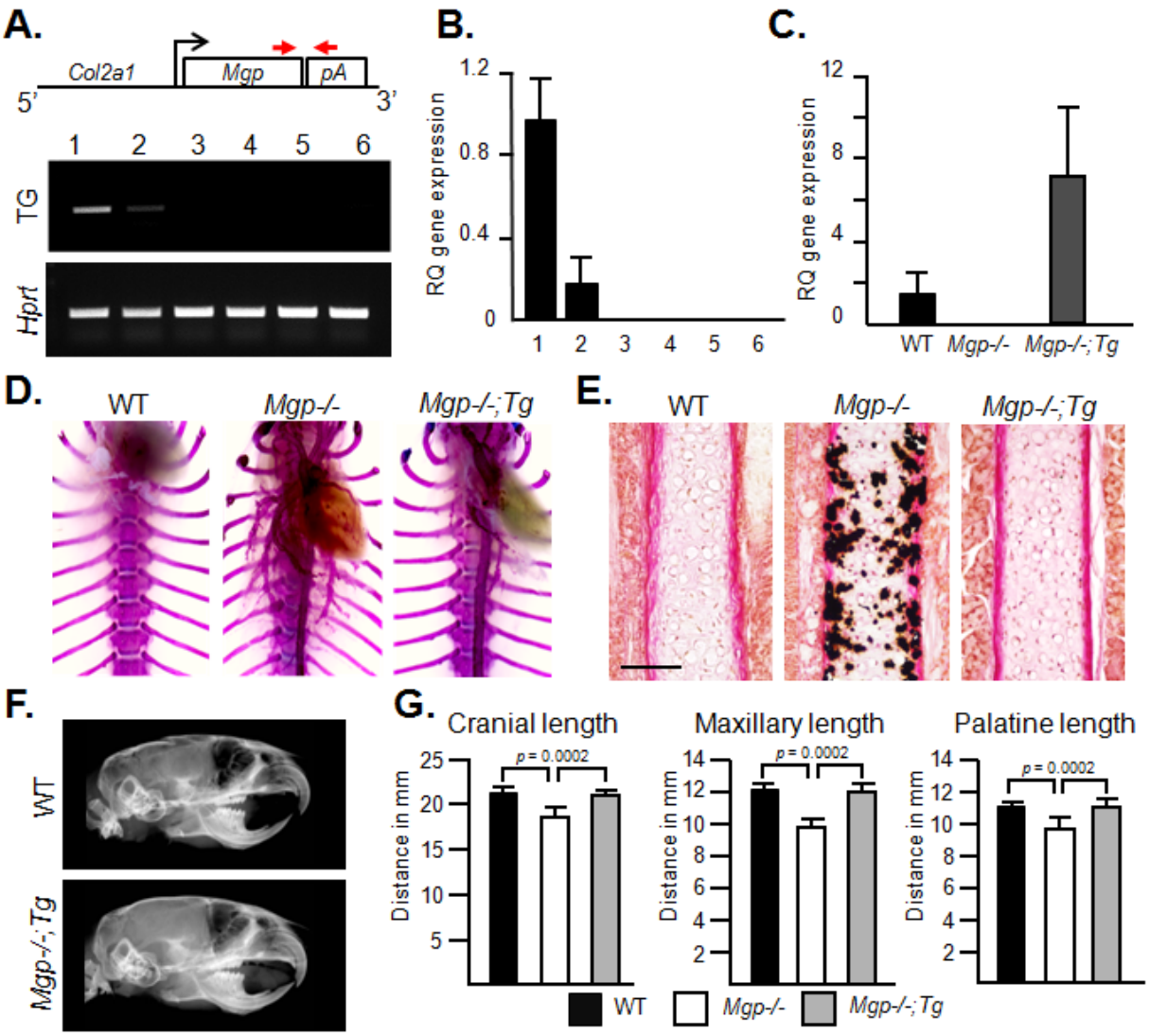

Figure 5: Local expression of *Mgp* in the cartilage corrects the midface hypoplasia in MGP-deficient mice. **A.** Schematic representation of genetic construct used to generate *Col2a1-Mgp* transgenic mice expressing *Mgp* under the cartilage-specific *Col2a1* promoter (top panel). The red arrows represent the primers used to detect the transgene by PCR. Semi-quantitative PCR showing the tissue-specific expression of the transgene in 2-week-old *Col2a1-Mgp* mice (middle panel, 1: Cartilage, 2: Aorta, 3: Calvaria, 4: Muscle, 5: Brain and 6: Long bone) showing a strong *Mgp* expression in cartilage and minor expression in aorta. **B.** qRT-PCR analysis of transgene expression in the same tissues described in Panel A. **C.** qRT-PCR showing approximately 6-fold increased *Mgp* expression in the nasal septum cartilage of *Mgp-/-;Col2a1-Mgp* (*Mgp-/-;Tg*) mice when compared with the WT littermates. Note the absence of *Mgp* expression in the nasal septum of *Mgp-/-* mice. **D.** Ribcage skeletal preparations of 5-week-old mice stained with alizarin red and alcian blue showing the vascular mineralization in *Mgp-/-* mice and in *Mgp-/-;Tg* mice. **E.** VKVG staining showing a complete absence of mineralization in the nasal septum of *Mgp-/-;Tg* mice. Scale bar represents 100μm. **F.** Lateral cephalic X-ray of WT and *Mgp-/-;Tg* littermates showing the correction of the craniofacial and dental phenotypes in the latter model. **G.** Craniofacial measurements showing the normalization of the cranial, maxillary and palatine lengths in *Mgp-/-;Tg* mice. Statistical analysis: ANOVA (Tukey's multiple-comparison test). All the analyses were done with 5-week-old mice (n=3 in each group for each experiment).

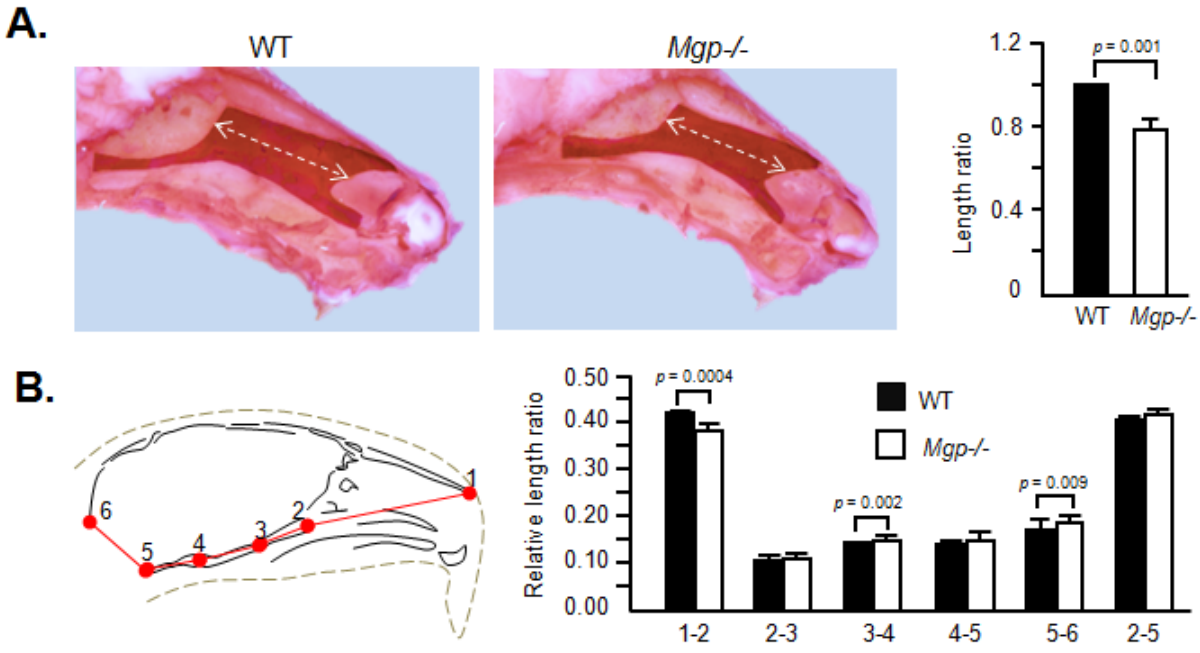

Figure 6: MGP-deficient mice have a shorter nasal septum. **A.** Exposed cartilaginous nasal septa of 5-week-old WT and *Mgp-/-* mice stained with Safranin O. Measurement of the lengths presented as relative length ratio shows a significantly smaller nasal septum in *Mgp-/-* mice. **B.** 2D cephalometric analysis of the viscerocranium and basicranium of 5-week-old WT and *Mgp-/-* mice. The viscerocranium (1-2) in *Mgp-/-* mice is significantly smaller when compared to WT mice, whereas the total basicranial length (2-5) is not affected. Values represent the ratio of the linear distance between points over the total cranial length (1-5). Description of the landmark's anatomical locations is presented in supplemental material Table S2, (n=5 in both groups). Statistical analysis: Student's *t* test in all cases.

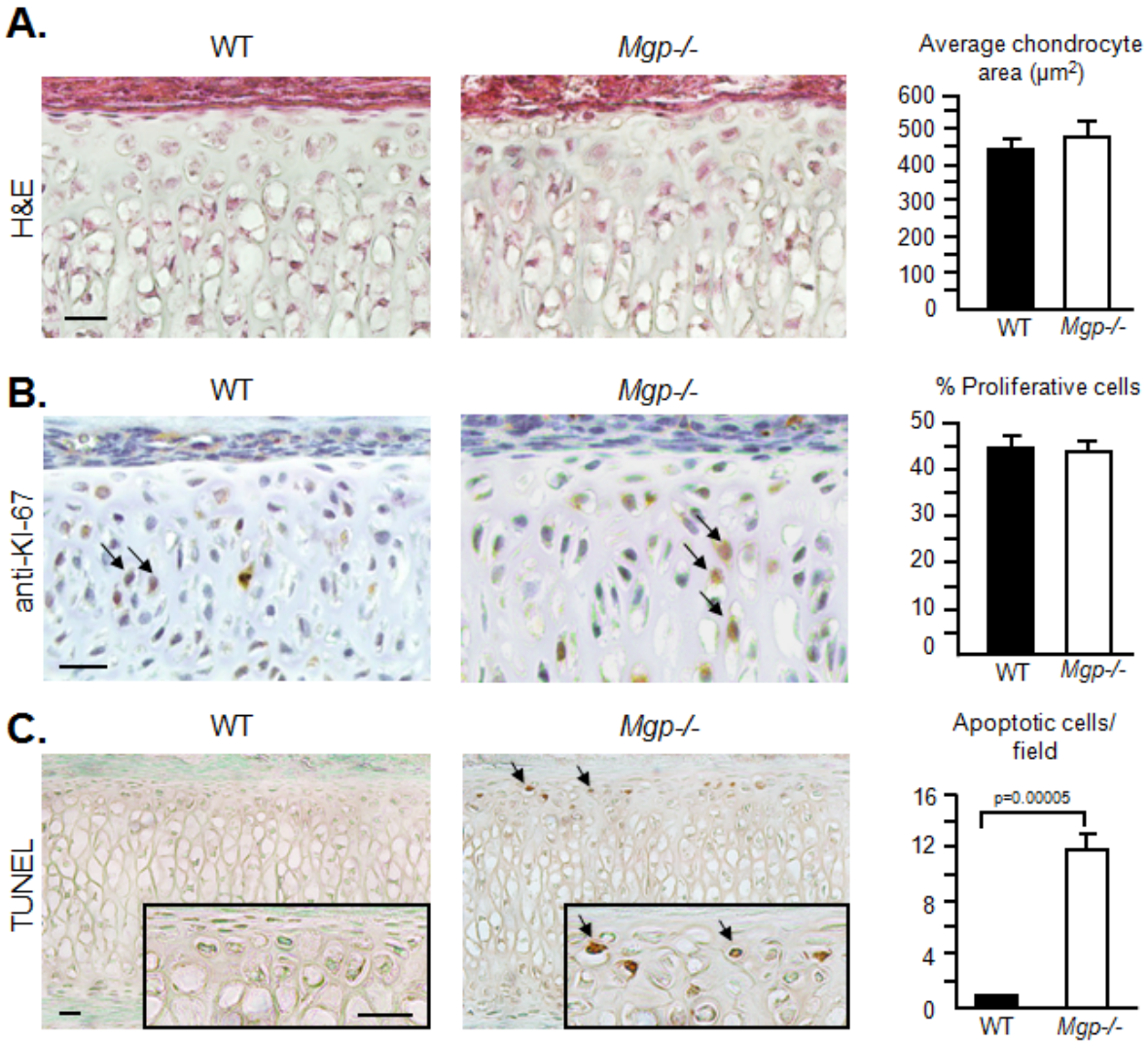

Figure 7: MGP-deficient septal chondrocytes undergo apoptosis. **A.** Quantification of cell area on histological sections of WT and *Mgp-/-* nasal septa stained with hematoxylin and eosin (H&E) shows no difference in chondrocyte size between the genotypes. Three fields were quantified per sample (n=3 in both groups). Scale bar represents 20μm. **B.** Anti-Ki67 antibody and hematoxylin staining of septal sections showing the proliferating chondrocytes (arrows). Quantification of proliferative cells/total cell count shows no difference between WT and *Mgp-/-* mice (n=6 in both groups). Scale bar represents 20μm. **C.** Colorimetric apoptosis detection assay (TUNEL) performed on WT and *Mgp-/-* septal sections shows the presence of apoptotic cells (arrow) in the MGP-deficient nasal septum but not in the WT nasal septum sections. The sections were counter-stained by methyl green (n=3 in both groups). Scale bars represent 20μm. All analyses were performed on 2-week-old mice; statistical analysis: Student's *t* test in all cases.

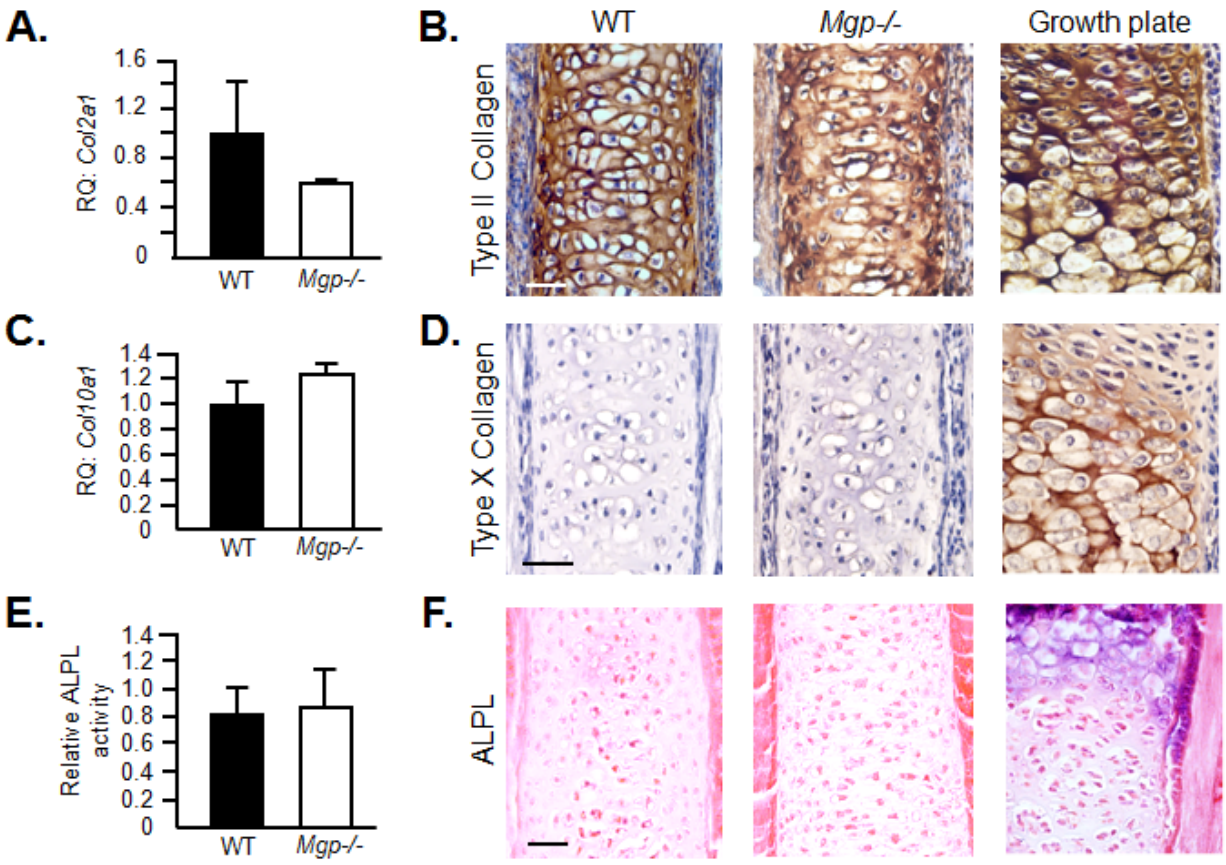

Figure 8: Chondrocyte hypertrophy is not a prerequisite for ectopic mineralization of the nasal septum in MGP-deficient mice. A. Gene expression analysis of *Col2a1* in 1-week-old WT and *Mgp-/-* nasal septa showing comparable expression in both groups. **B.** Immunohistochemistry showing similar expression pattern of type II collagen in 2-week-old WT and *Mgp-/-* nasal septa. Embryonic humerus growth plate staining was used as a positive control. **C.** *Col10a1* gene expression in 1-week-old WT and *Mgp-/-* mice showing no induction in the 'knockout' tissue. **D.** Absence of anti-Type X collagen staining in the WT and *Mgp-/-* 2-week-old nasal septum. Embryonic humerus growth plate staining was used as a positive control. **E.** The alkaline phosphatase (ALPL) basal activity in *Mgp-/-* nasal septum extracts from 2-week-old mice is comparable to that of WT littermates. **F.** ALPL staining confirms the absence of ALPL activity in the septal cartilage of *Mgp-/-* mice. Staining of septal growth plate sections from 2-week-old WT mice was used as a positive control. Scale bars for histological sections represent 40μm. Statistical analysis: Student's *t* test in all cases.

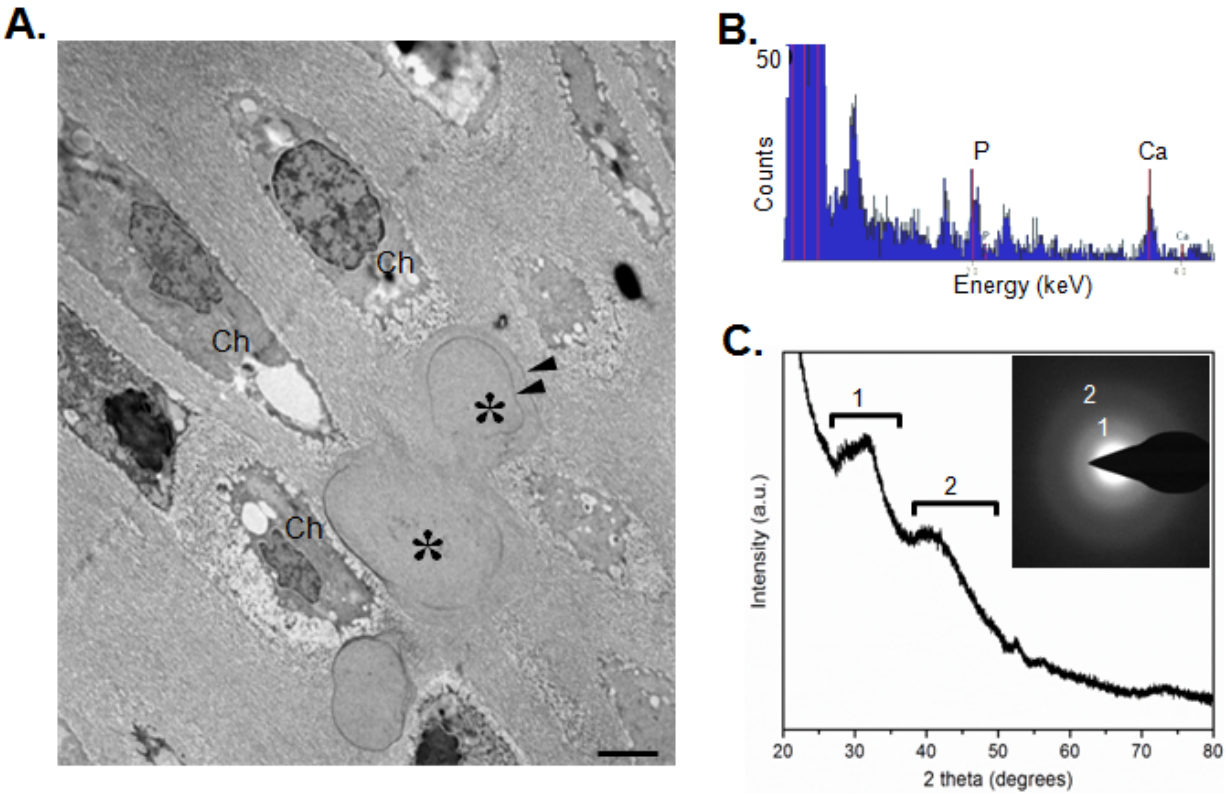

Figure 9: Amorphous calcium phosphate as main mineral species in MGP-deficient nasal septum. A. Transmission electron microscopy of 1-week-old *Mgp-/-* nasal septum showing the presence of chondrocytes (Ch), and mineral deposits (asterisks) having an unusual globular shape. Note the incremental lines (suggesting periodic mineral deposition) within the mineral deposits (arrowheads). **B.** Energy-dispersive X-ray spectroscopy showing the presence of phosphorus and calcium within the mineral deposits. **C.** X-ray diffraction showing that the mineral phase is largely amorphous calcium phosphate. Minor spectral peaks labelled 1 and 2 indicate tendencies toward crystallization (initiation) of an apatitic phase. **Inset in C.** Electron diffraction pattern confirming the presence of mostly amorphous mineral showing only diffuse (rather than sharp) electron diffraction rings labelled as 1 and 2 (n=3 mice for each group and each experiment).

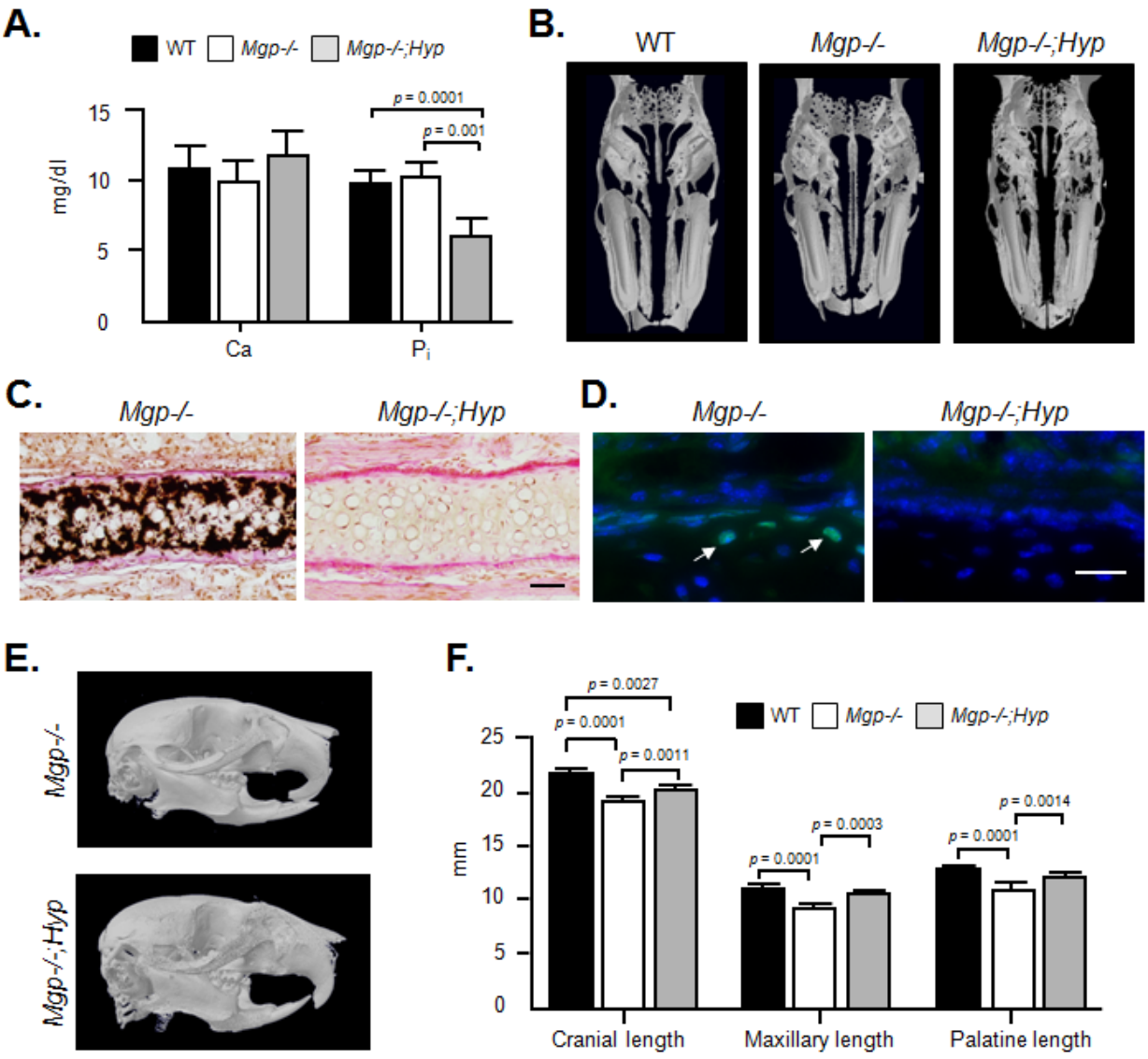

Figure 10: Prevention of nasal septum mineralization in *Mgp-/-;Hyp* mice. **A.** Serum calcium and inorganic phosphate levels in the WT, *Mgp-/-* and *Mgp-/-;Hyp* mice show similar calcium levels in all the genotypes and confirms the presence of hypophosphatemia in the *Mgp-/-;Hyp* mice. Values are shown in mg/dl. (n=4). **B.** 3D reconstruction of micro-CT scans of gender- and age-matched WT, *Mgp-/-* and *Mgp-/-;Hyp* mice showing the correction of nasal septum mineralization in the double mutant. **C.** Histology of nasal septum of *Mgp-/-* and *Mgp-/-;Hyp* mice stained with VKVG confirming the absence of apatitic minerals in the latter phenotype. Scale bar represents 50μm. **D.** Fluorometric TUNEL assay shows the presence of apoptotic immature chondrocytes in 3-week-old *Mgp-/-* (arrows), but not in *Mgp-/-;Hyp* nasal septa. Images of the same field showing fluorescein-12-dUTP (labels fragmented DNA ends) and H33258 (nuclear stain) fluorescence were overlaid to create the combined images. Scale bar represents 25μm. **E.** 3D reconstruction of micro-CT scans of *Mgp-/-* and *Mgp-/-;Hyp* mice. Note the correction of the midface hypoplasia and class III malocclusion in the compound mutant. **F.** Cephalometric analysis of WT, *Mgp-/-* and age- and gender-matched *Mgp-/-;Hyp* mice showing a complete correction of the palatine and maxillary lengths in the *Mgp-/-;Hyp* mice. Although the cranial length is corrected in the *Mgp-/-;Hyp* mice when compared to *Mgp-/-* mice, it remains shorter than the WT controls. All the analyses were performed in 5-week-old mice unless indicated otherwise (n=3 male mice in each group for each experiment). Statistical analysis: ANOVA (Tukey's multiple-comparison test).

Matrix Gla Protein Deficiency Impairs Nasal Septum Growth Causing Midface Hypoplasia

Juliana Marulanda, Hazem Eimar, Marc D McKee, Michelle Berkvens, Valentin Nelea, Hassem Roman, Teresa Borrás, Faleh Tamimi, Mathieu Ferron and Monzur Murshed

J. Biol. Chem. published online May 9, 2017
